Scanning Tunneling Microscopy, Orbital-Mediated Tunneling Spectroscopy, and Ultraviolet Photoelectron Spectroscopy of Nickel(II) Octaethylporphyrin Deposited from Vapor

L. Scudiero, Dan E. Barlow, and K. W. Hipps*

Department of Chemistry and Materials Science Program, Washington State University, Pullman, Washington 99164-4630

Received: June 26, 2001; In Final Form: September 19, 2001

Thin films of vapor-deposited Ni(II) octaethylporphyrin (NiOEP) were studied supported on gold. Thin films thermally deposited onto flame-annealed Au (111) were analyzed by ultraviolet photoelectron spectroscopy (UPS) using He I radiation and by X-ray photoelectron spectroscopy (XPS) using Mg Kα radiation. Reflectance absorption infrared spectroscopy (RAIRS) was used to study NiOEP films on polycrystalline gold. Scanning tunneling microscopy (STM) and orbital-mediated tunneling spectroscopy (STM-OMTS) were performed on submonolayer films of NiOEP supported on Au(111). The highest occupied π molecular orbitals of the porphyrin ring were seen in both STM-OMTS and in UPS at about 6.4 and 6.8 eV below the vacuum level. The lowest unoccupied π^* molecular orbital of the porphyrin ring also was observed by STM-OMTS to be located near 3.4 eV below the vacuum level.

Introduction

Metalloporphyrins are intensively studied for many reasons. They play an important role in a wide variety of biological processes ranging from oxygen transport to pigmentation changes. They can act as catalysts,[1] and there has been significant recent interest in structural distortions from planar geometry.[2−35] Metalloporphyrins can undergo reversible redox reactions in which the site of electron transfer may be localized on the porphyrin ring, or on the central metal ion. Both reaction types are important in natural processes.[6] Thin porphyrin films on metal and semiconductor surfaces are also of great interest. Chemical sensors made from porphyrin films have been reported.[7] In the electrochemical environment, infrared (IR) spectroscopy,[6] Raman spectroscopy,[8] and scanning tunneling microscopy (STM)[9−15] studies have provided a wealth of information on the structure of porphyrins at the electrode surface. Langmuir−Blodgett films,[16] self-assembled monolayers,[9,17] and self-organized structures[18,19] of porphyrins have been studied by a wide variety of techniques. Vapor-deposited porphyrins have received less attention.

IR transmission spectra and electron diffraction studies have been performed on thin films of metal free tetraphenylporphyrin (H_2TPP) vapor deposited onto KCl.[20] Ultrahigh-vacuum (UHV) studies of vapor-deposited Cu(II) tetra-(3,5-di-tertiary-butylphenyl) porphyrin (CuTTBPP) on Cu(100) have been reported by Gimzewski,[21,22] who has also provided a single image of a mixed monolayer of CuTPP and CuTTBPP on Cu(100).[22] Recently, Scudiero et al. reported an XPS, IR, STM, and STM orbital-mediated tunneling (STM-OMT) study of submonolayer films of CoTPP and NiTPP on Au(111) under UHV conditions.[23,24]

Scudiero et al. analyzed IR and XPS spectra of thin films of Co(II)TPP, Cu(II)TPP, and Ni(II)TPP in terms of oxidation state, chemical composition, and orientation.[23] It was found that these compounds may be thermally deposited onto gold without change in chemical composition or oxidation state. Molecular resolution STM images were reported and chemical specificity in STM imaging for these complexes was demonstrated.[23,24] As had been previously shown for metal phthalocyanine (MPc) complexes,[25−27] varying the metal ion at the center of a metal-(II) tetraphenylporphyrin (MTPP) produced huge variations in the constant current STM images. This was interpreted as indicating large changes in tunneling probability associated with occupancy of the d_{z^2} orbital of the transition metal ion. Scudiero et al. also provided electronic spectroscopic properties of metallotetraphenylporphyrins.[24] In particular, they determined the energies of the highest occupied and lowest unoccupied π orbitals, and the highest occupied d metal orbital. For the first time, results from STM and tunnel-diode-based orbital-mediated tunneling spectroscopy, and from ultraviolet photoemission spectroscopy (UPS) measurements on the same species were reported and compared. All three types of spectra were in agreement in their regions of overlap.[24] An electrochemical model for estimating orbital-mediated tunneling bands was found to give good qualitative agreement with experiment, and good quantitative agreement for transient reduction processes and oxidative processes near the Fermi energy E_F. The quantitative predictions of the model were poor for oxidative processes far from E_F.

In the present study attention is turned to a different metalloporphyrin, Ni(II) octaethylporphyrin (NiOEP). A space filling model (CPK) of a typical first row M(II)OEP is shown in Figure 1 in both top and side views. This model is based on the crystal structure of NiOEP,[28] but with the ethyl groups all curled in the same direction. This configuration was chosen because it is consistent with the STM images we have obtained (vide infra). In the crystal, four curl up and four curl down. NiOEP offers the possibility of a significant change in geometry for the adsorbed species relative to the nickel tetraphenylporphyrin (NiTPP). Consider NiTPP and NiOEP adsorbed on Au-(111). Because the phenyl groups of NiTPP are roughly perpendicular to the porphyrin ring, they force the central ring plane to lay about 0.34 nm above the gold surface. NiOEP, on the other hand, can have the porphyrin ring in direct contact with the metal surface by adopting the conformation shown in

* To whom correspondence should be addressed. E-mail: hipps@wsu.edu.

10.1021/jp012436m CCC: $22.00
Published on Web 11/02/2001

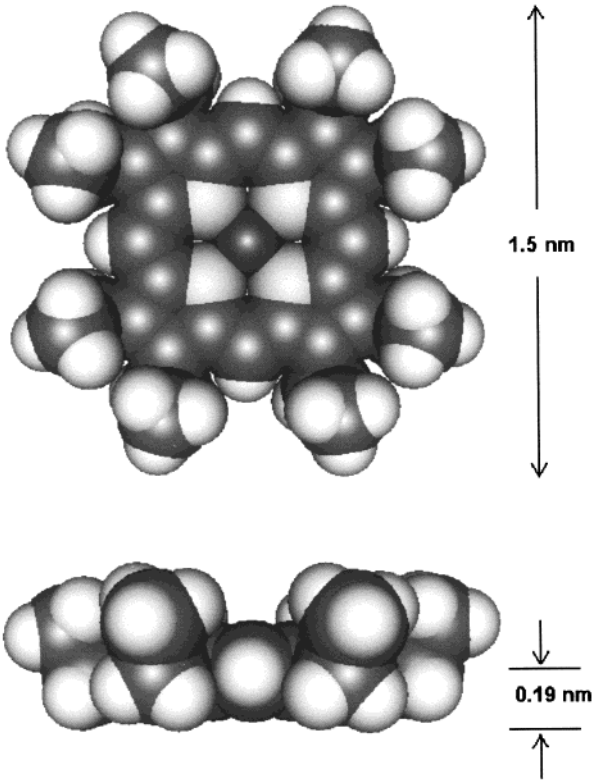

Figure 1. CPK model of a typical metal(II) OEP. The four nitrogens that bind the central metal ion are shown in light gray. The molecule is shown both in top and side view. The configuration of the ethyl groups is chosen to be consistent with the structure of NiOEP adsorbed on Au(111).

Figure 1. The present paper was motivated by our desire to understand the effects on conformation and electronic structure of this potentially stronger interaction between NiOEP and Au(111). XPS and Fourier transform infrared (FT-IR) spectroscopy (RAIRS and transmission modes) will be used to establish that the chemical composition of NiOEP thermally deposited on gold is unchanged by the preparation process. UPS and STM-based orbital-mediated tunneling spectroscopy (STM-OMTS) will be used to probe the highest occupied and lowest unoccupied molecular orbitals.

To contrast and compare experimental results from STM-OMTS and UPS, we will utilize the energy of the vacuum level (zero kinetic energy electron) as a unifying reference point. STM-OMTS data are conventionally presented with the zero taken at the Fermi level E_F and peak positions are reported as shifts (Δ_o and Δ_r). Once E_F is determined, however, these can be converted to energies below the vacuum level as shown in Figure 2. Similarly, ultraviolet photoelectron spectroscopic determination of occupied orbital energies are normally measured relative to the Fermi energy and these binding energies can also be converted (using Figure 2) into ionization energies I (orbital energies below the vacuum level). Electron affinities A, the energy gained by adding an electron to an unoccupied orbital, also are given conventionally relative to the vacuum level. Reduction and oxidation potentials in solution, often given relative to sce, may also be converted to energies below the vacuum level by using a procedure given by Richardson.[29] Key to many of these conversions is a knowledge of the Fermi energy relative to the vacuum level. The Fermi energies for the gold samples used in this work were determined in a previous paper[24] and will be used to convert the variously measured quantities to energies below the vacuum level.

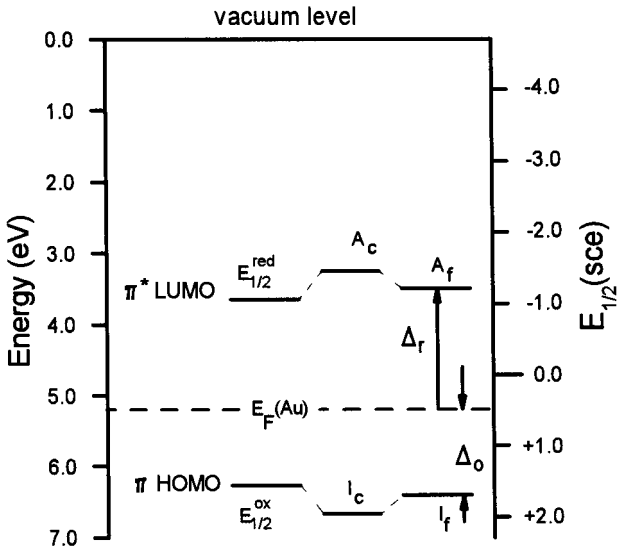

Figure 2. Schematic of critical energy levels of a porphyrin relative to the vacuum level, standard calomel electrode (sce), and Fermi energy. A_c and A_f are electron affinity levels for crystalline and for thin film on metal phases, respectively. A is the energy required to take an electron from a negative ion state to the vacuum level and leave a neutral molecule. I_c and I_f are the corresponding ionization energies and are the energies required to take an electron from an orbital of a neutral molecule to the vacuum level.

Experimental Section

Materials. Metalloporphyrins were purchased from Porphyrin Products and used as supplied. NiOEP was sent to Desert Analytics for elemental analysis and the results were (C) 73.1% expected, 73.4% found; (H) 7.5% expected, 7.3% found; (N) 9.5% expected, 9.5% found. Gold and aluminum metals were >99.99% purity. The porphyrins were deposited from Ta metal sources for all STM, XPS, and UPS samples, while a quartz crucible was used for RAIRS sample preparation.

STM Sample Preparation and Data Acquisition. Epitaxial Au(111) films with well-defined terraces and single atomic steps were prepared on mica by previously described methods.[25,27] These films were 0.1−0.2 μm thick and had a mean single grain diameter of about 0.3 μm. Unlike true single-crystal gold,[30] these small crystal grains showed reconstruction line spacing ranging from 6.3 to about 9.0 nm. The gold films were transferred via air-lock into the UHV STM chamber (working pressure $\sim 5 \times 10^{-10}$ Torr) where the porphyrin was thermally deposited and then studied without exposure to air. The thickness of the metalloporphyrin layers was determined with a quartz crystal thin film monitor. The STM head used was produced by McAllister Technical Services (Coeur d'Alene, ID) and is of the inertial approach type. A Digital Instruments Nanoscope III controller was used to acquire and process the reported data. Constant current images are reported and any filtering is indicated in the appropriate figure caption. All images were acquired at about 21 °C. Both etched W and cut $Pt_{0.8}Ir_{0.2}$ tips were used. Generally, the tips required a UHV cleaning step (electron beam bombardment) in order to produce high-quality images. Spectroscopy was performed by using the Digital Instruments software to measure current as a function of sample bias voltage $I(V)$ at fixed tip−sample separation (feedback off). $I(V)$ curves were recorded for different x and y coordinates, where x and y were manually changed by steps of 1 nm. The resulting curves were then averaged and dI/dV was obtained as a numerical derivative of the average $I(V)$. The dI/dV data presented here are the average of 8 to 12 spectra. STM spectra

(d*I*/d*V* at fixed height) were measured both on islands of the porphyrin and over the clean gold surface as pairs. Spectra having anomalous structure over gold indicated that tip artifacts were present and both the porphyrin and the Au surface d*I*/d*V* curves were discarded.

IR Sample Preparation and Spectral Acquisition. In a glass bell jar deposition system (base pressure $\sim 7 \times 10^{-8}$ Torr) 200 nm of Al was first deposited on clean glass microscope slides. Then, about 30 nm of Au was deposited at a rate of 0.17 nm/s on the Al film. Three such substrates were made at one time. On two of these substrates, 24 nm (as determined by a quartz crystal microbalance) of NiOEP was deposited at a rate of 0.2 nm/s. A density of 1.3 g/cm^3 was assumed. The third substrate was used as the RAIR reference. Substrates were maintained near 21 °C during NiOEP deposition. Samples and reference were then removed from the deposition system and transferred to the vacuum (roughing pressure) bench of a Bruker IFS113 Fourier transform IR spectrometer. These samples were studied by reflectance-absorption IR (RAIR) with an 86° angle of incidence. Alternatively, <1 mg of metalloporphyrin was thoroughly ground with 100 mg of KBr and pressed into a pellet. A pure KBr pellet was used as a reference. These samples were measured in transmission mode in the same (IFS113) spectrometer.

For all IR measurements, a globar source, Ge-coated KBr beam splitter, and a wide band LN2-cooled HgCdTe detector were used. The bench pressure was maintained below 20 mTorr throughout the measurement cycle. RAIRS spectra were acquired at an angle of incidence of 86° and 8 cm^{-1} resolution (two data points per resolution interval). Typical RAIRS spectra are the result of 8000 scans. Transmission IR spectra were also obtained with 8 cm^{-1} resolution and 256 scans were averaged. All IR data are reported in absorbance units.

UPS Sample Preparation and Data Acquisition. UPS data were obtained with a homemade He lamp source which produces two resonance lines, He I (21.2 eV) and He II (40.8 eV), by cold cathode capillary discharge. The He I lamp was set to run with a filament current of 17 A and voltage of 9 V and He gas pressure of 250 mTorr. The discharge was adjusted to 190 V and 0.5 A. Only the 21.2 eV He I line was used in this study. A platinum-coated concave 600 groove/mm reflection grating with a 3.5° blaze angle coupled with a gold-coated spherical focusing mirror was used to produce monochromatic UV radiation. The base pressure in the monochromator chamber was 2×10^{-9} Torr. The UPS system is attached via a UHV valve to a Kratos Axis-165 electron spectrometer having a base pressure of 5×10^{-10} Torr.

Two different types of gold surfaces were studied. Au(111) samples (140 nm thick) made in a vacuum ($<3 \times 10^{-9}$ Torr) by vapor deposition on mica[26] and flame-annealed Au(111). The Au(111) samples were prepared exactly as described for the STM substrates, above. Both types of gold were used to check the substrate work function and the calibration of the He lamp. In addition, the flame-annealed gold sample was used as the substrate for the porphyrin UPS studies. NiOEP was thermally deposited onto flame-annealed Au (111) in a vacuum (5×10^{-9} Torr) prep chamber attached to the UPS spectrometer. The thickness of the porphyrin samples was 4 nm as determined with a quartz crystal microbalance and using a density of 1.3 g/cm^3.

The UPS were acquired using an electrostatic lens that focused the ejected electrons into the Kratos spectrometer. A bias of −20 V was applied to the sample to shift the spectra out of the nonlinear region of the analyzer (KE = 0−10 eV).

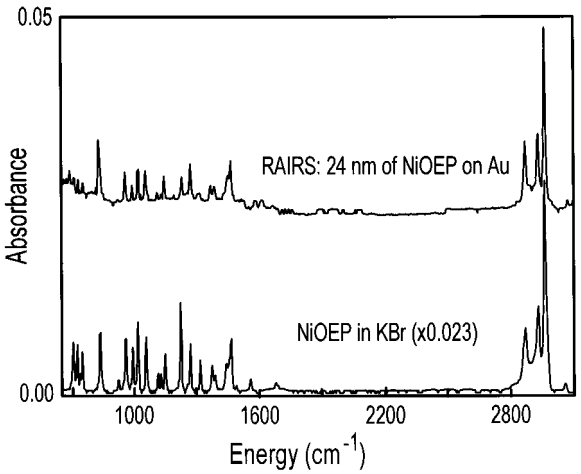

Figure 3. Transmission and RAIRS spectra of NiOEP. The transmission spectrum of ca. 1% NiOEP in KBR is the lower trace. The upper trace is the RAIRS of 24 nm of NiOEP deposited on polycrystalline gold.

The spectrometer was used in fixed analyzer transmission mode with a pass energy of 20 eV and spatial resolution of 120 μm. The photoemitted electron energies were analyzed by a Kratos hemispherical analyzer and counted by eight channel electron multipliers. Under these conditions the energy resolution of the spectrometer is better than 150 meV, which was determined at the Fermi edge of an Ar-etched single crystal of Au (111).

XPS Sample Preparation and Spectral Acquisition. XPS samples of porphyrin were prepared with the same procedures as for the UPS samples producing 4 nm and 0.5 nm thickness films on flame-annealed Au (111). Achromatic X-radiation (280−300 W) at energy 1253.6 eV (Mg Kα) was used as XPS excitation sources. The analyzer was set for a spatial resolution of 120 μm. The energy resolution was set to 1.3 eV for survey spectra, and to 0.8 eV for the higher resolution acquisitions of C 1s, N1s, Ni 2p, and Au $4f_{7/2}$ peaks. Binding energies were calibrated against the Au $4f_{7/2}$ peak taken to be located at BE = 84.3 eV. The attenuation of the Au line by the thin film was used to correct the C 1s peak before quantifying the elements because some carbon (<1% mass concentration) was present on the Au reference samples. The intensity ratio of the C 1s to Au $4f_{7/2}$ lines before NiOEP deposition was scaled by the Au $4f_{7/2}$ intensity after deposition and then subtracted from the overall C 1s intensity.

Results and Discussion

Infrared Spectroscopy. Figure 3 shows the RAIR spectrum of a 24 nm thick film of NiOEP on Au and the transmission IR spectrum of NiOEP powder supported in a KBr pellet. Peak positions and assignments are collected in Table 1, where the assignments were taken from the work of Nakamoto and Spiro.[31,32,33] The various carbon atoms referenced in Table 1 are identified in Figure 4, a sketch of a repeating segment of the OEP ligand. Although relative peak intensities vary due to differences in selection rules and orientations, there is good agreement between the peak positions observed in the thin film and bulk samples. The metal sensitive bands are located near 1229, 993, 922, and 748 cm^{-1}, with shifts of 10 to 15 cm^{-1} resulting from substitution of Mn or Zn for Ni. Oxidation or reduction of the metal ion or ligand can result in peak shifts of the order of $\pm$ 10 cm^{-1}.[34,35] Thus, the RAIRS data suggest that NiOEP can be thermally deposited without decomposition or change in oxidation state. Note, that these statements about

TABLE 1: Peak Positions and Assignments for NiOEP RAIRS Bands (thin film) and Transmission Spectrum in a KBr Pellet[a]

thin film	in KBr	assignment[b]
2962	2961	ν (CH) ethyl group
2928	2928	ν (CH) ethyl group
2868	2868	ν (CH) ethyl group
	1556	ν ($C_\alpha C_m$)
1463	1464	δ (CH_3) ethyl group
1449	1441	ethyl group
1385	1387	ν ($C_\alpha C_\beta$) $-$ ν ($C_\beta C_1$)
1367	1372	ethyl group
1307	1314	ethyl group
1270	1268	ν ($C_\alpha N$), δ ($C_\alpha C_m H$)
1228	1223	ν ($C_\alpha C_m$), ν ($C_\alpha N$), δ ($C_\alpha C_m H$)
1144	1148	ν ($C_\alpha N$), δ ($C_\alpha C_m H$)
1129	1126	ν ($C_\alpha N$), δ ($C_\alpha C_m H$)
1112	1112	ethyl group
1055	1056	ethyl group
1019	1018	ethyl group
991	992	ν ($C_\alpha C_m$), ν ($C_\beta C_1$)
954	957	ethyl group
922	922	ν ($C_\alpha C_m$), ν ($C_\beta C_1$)
830	832	π ($C_m H$)
753	748	δ ($C_\beta C_1 H$) + δ ($C_2 C_1 H$) ethyl
728	723	δ ($C_\beta C_1 H$) + δ ($C_2 C_1 H$) ethyl + δ ($C_\alpha C_\beta N$)
710	704	π (skeletal)

[a] Values are in cm^{-1} ± 3 cm^{-1}. [b] Assignments are based on refs 31, 32, and 33. The designation C_α , C_β, C_m, C_1, and C_2 refer to the carbon atoms adjacent to the nitrogen atom, at the β pyrrole position, the methine bridges and the substituent, respectively. The symbols ν, δ, and π refer to stretching, bending, and out-of-plane bending. See Figure 4 for clarity.

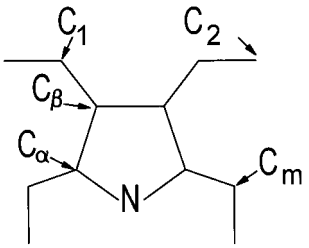

Figure 4. Sketch of a fragment of octaetylporphyrin indicating the labeling of carbon atoms as they appear in Table 1.

chemical stability concern the thermal deposition and NiOEP on NiOEP film growth. The films are too thick to allow conclusions concerning the Au/NiOEP interface. It is also important to note that the 24 nm film is of the order of 20 monolayers thick and is therefore almost certainly a textured nanocrystalline film. The orientation of the NiOEP units within this film will not necessarily (and in fact almost certainly do not) match the structure of a monolayer film. The presence of both out-of-plane (π type) and in plane (ν and δ type) modes in the spectrum obtained from a 24 nm film clearly indicate that the molecules are neither simply parallel or perpendicular to the metal surface. They are either oriented at an angle with respect to the normal, or occur in domains of differing orientation.

XPS Results. Table 2 collects the peak positions and relative atomic percent concentrations of the principal XPS peaks for carbon, nitrogen, and nickel observed in this study. Because of the increased uncertainty due to noise, quantification is only reported for the 4 nm film. For comparison, values reported for the C1s and N1s lines in H_2OEP[36] and the Ni $2p_{3/2}$ in NiOEP[37] are also given. Note that the 0.5 nm thick film is very nearly one monolayer as determined by the space filling models. Both the positions and percentage composition indicate that NiOEP can be thermally deposited onto gold without change of composition or oxidation state. It is also interesting to note that the C 1s lines due to the ethyl groups are sufficiently shifted to be seen as a well-defined shoulder on the ring carbon peak. There is no evidence in the XPS of redox processes between the Au substrate and the NiOEP. Changes in oxidation state of the Ni(II) ion would have produced shifts of about 1.8 eV in the $2p_{3/2}$ peak, and reduction of the ring would result in shifts of about 0.6 eV in the C1s peak.[38] The 0.5 nm film is sufficiently thin so that strong interactions (e.g., electron transfer) between the gold surface and the NiOEP would be discerned as clear shifts in the observed peaks. Thus, the XPS and RAIR data demonstrate that NiOEP can be thermally deposited without change in chemical composition, and the XPS data show that it can be deposited onto gold without decomposition or change in oxidation state.

STM Imaging. Figure 5 is a typical constant current image of NiOEP on Au(111) observed at low resolution. In this image the individual NiOEP molecules appear as dots making up well-defined single molecule thick islands (e.g., region A). The regions between the islands (e.g., region B) appear to be uncovered Au(111) surface and the $I-V$ curves obtained in these regions are similar to those from porphyrin free substrates. The large height step (feature C) along the lower right side of the figure is due to a monatomic step of the Au(111) substrate. One can also observe striations running through both the NiOEP islands and portions of the uncovered surface. These are due to reconstruction of the Au(111) surface and appear as pairs of lines. The small grain gold films used in this study (about 0.3 μm in diameter) generally have a larger reconstruction line spacing than is seen on large single-crystal Au(111) surfaces. Unlike true single-crystal gold,[30] these small crystal grains show reconstruction line spacing ranging from 6.3 to about 9.0 nm.

TABLE 2: Peak Positions (Binding Energy in eV) Obtained by XPS Using MgKα[a]

NiOEP (4 nm)	element	peak position (this work)	peak position (reported)	measured relative[d] concentration	theoretical relative[d] concentration
low resolution (1.3 eV)	C1s	284.7	284.6[b]	1.00	1.00
	N1s	398.7	398 $\pm$ 1[b]	0.11	0.11
	Ni $2p_{3/2}$	854.7	854.8[c]	0.027	0.028
high resolution (0.8 eV)	C1s	284.7	OEP ring	1.00	1.00
	C1s	285.6	ethyl group	0.81	0.80
	N1s	398.8		0.19	0.20
	Ni $2p_{3/2}$	855.1	854.8[c]	0.047	0.05
NiOEP (0.5 nm)	C1s	284.4			
	C1s	285.5			
	N1s	398.7			
	Ni $2p_{3/2}$	855.1			

[a] The Au $4f_{7/2}$ line at 84.3 eV was used as reference. [b] Values for H_2OEP taken from ref 36. [c] Value for NiOEP taken from ref 37. [d] Ratio of atomic concentration of given species to that having C 1s peak at 284.7 eV.

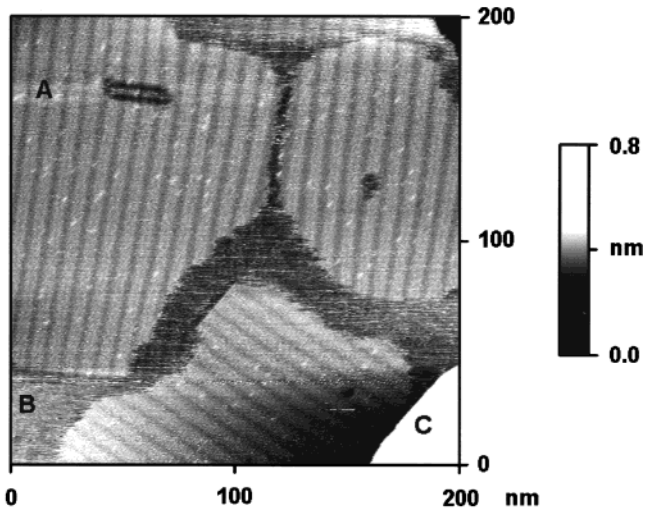

Figure 5. A typical constant current image of NiOEP on Au(111) observed at low resolution. The image was obtained with a W tip at a sample bias voltage of −1.2 V and a set point of 300 pA. The image has been flattened. The region marked B is uncovered Au(111) and the region marked A is a single molecule thick layer of NiOEP. The area marked C is a single gold atomic step.

Figure 6 is a high-resolution image of NiOEP on Au(111) that clearly shows the 4-fold symmetry expected for the molecule and the somewhat dark center associated with the central Ni(II) ion. The metal ion contrast has been explained in terms of occupation of the d_{z^2} orbital.[23−27] Also shown as an inset in Figure 6 are space filling (CPK) models of NiOEP placed to form a single primitive surface unit cell with basis vectors of length 1.65 and 2.76 ± 0.20 nm. Note that there are 2 molecules per unit cell because of the small angular offset (ca. 15°) of alternating rows. Another interesting aspect of the NiOEP image is the prominence of the ethyl groups. While the individual hydrogens cannot be resolved, the terminal methyl groups are clearly seen with contrast similar to, but slightly greater than, the OEP ring. Moreover all the ethyl groups are turned up so that there is maximal contact between the OEP ring and the gold surface (as shown in Figure 1).

The mechanism by which the ethyl groups attain their prominence in the STM image is of interest. The porphyrin ring shows good contrast because of both HOMO- and LUMO-mediated tunneling in the energy region close to E_F (vide infra). One might expect, however, that the oxidation and reduction processes that change electron density in the ethyl groups should be located several eV from E_F, thereby giving the ethyl groups a low effective height. This expectation is apparently an oversimplification of the electronic states associated with the ethyl groups. Li et al.[31] have observed that C−C stretching and C−H bending bands associated with the ethyl groups of NiOEP are surprisingly strong in resonance Raman spectra. They determined that this indicates an appreciable involvement of the ethyl groups in the porphyrin $\pi-\pi^*$ excited states. Thus, changes in oxidation state of the porphyrin ring might well translate into changes in electron density on the ethyl groups.

Ultraviolet Photoemission Spectroscopy (UPS). In general, the photoemission process is described by the following expression:

$$M_0 + h\nu \rightarrow M_j^+ + e^-$$

The ionization energy to produce state j of the positive ion M^+ is expressed by

$$I_j = h\nu - KE_j \qquad (1)$$

where I is the ionization energy measured relative to the vacuum level, KE is the kinetic energy of the ejected photoelectron, and $h\nu$ is the energy of the photon. Often, because of experimental

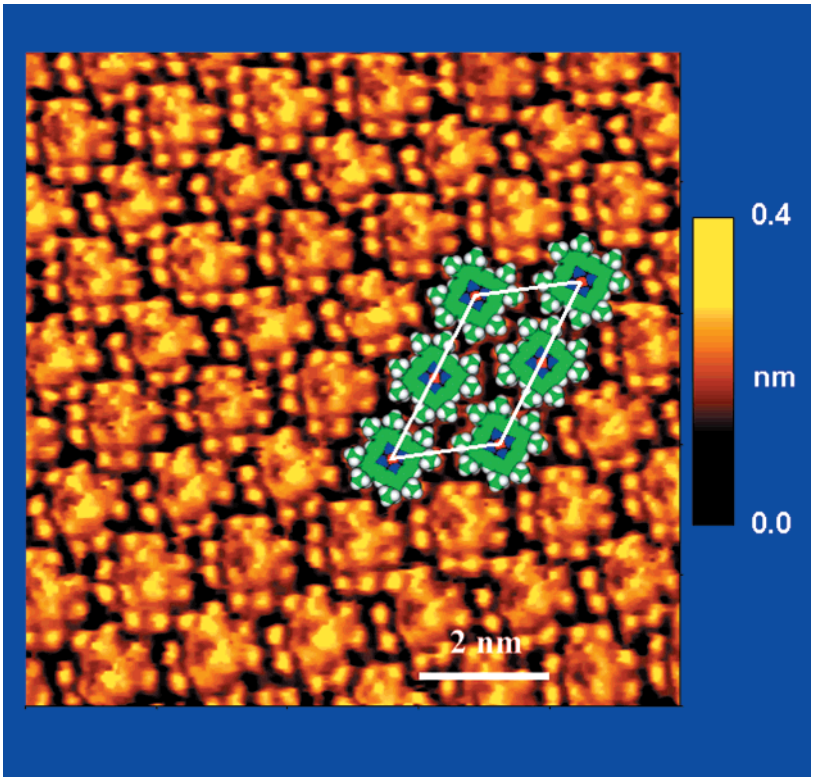

Figure 6. High-resolution constant current STM image of NiOEP at near-monolayer coverage on Au(111). The image was acquired with a W tip at −0.6 V bias, with a setpoint of 0.3 nA. The image was flattened and low-pass filtered. Inset is a group of CPK models arranged as a single unit cell.

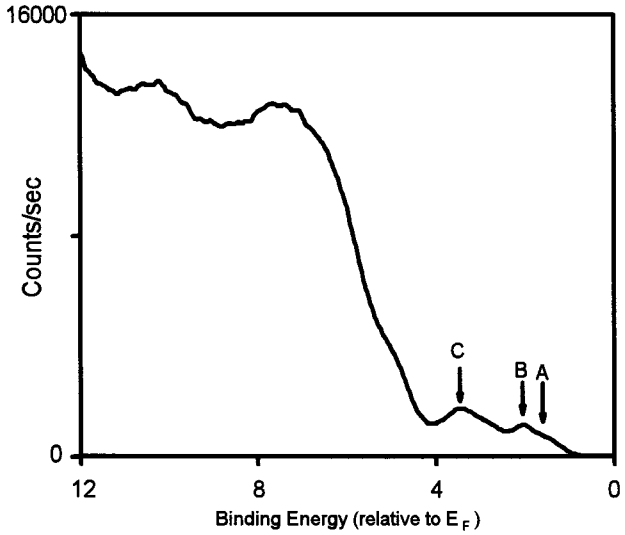

Figure 7. Raw UPS data obtained from a 4 nm film of NiOEP vapor deposited on a flame-annealed Au (111)gold surface. HeI radiation was used. The peaks marked A, B, and C are located at 1.6, 2.1, and 3.4 eV below the Fermi energy.

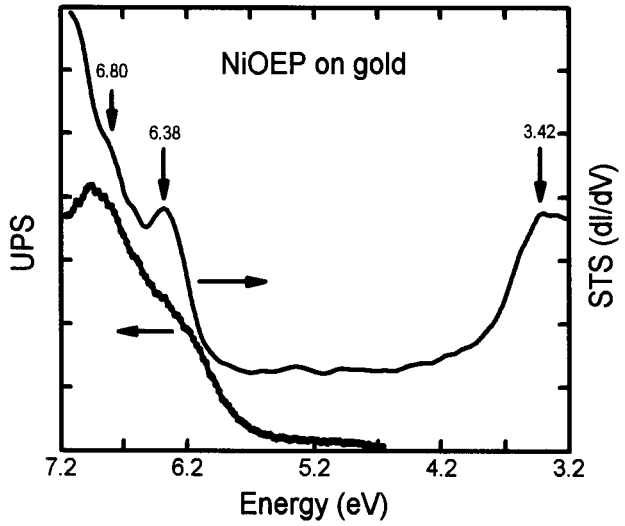

Figure 8. Combined results of UPS and STM-OMTS obtained from NiOEP deposited on Au(111). Curve positions on the *x*-axis are adjusted for differences in device work function. The STM d*I*/d*V* data were acquired from a 0.1 nm thick NiOEP film on Au(111) using a tungsten tip at a fixed height consistent with 0.3 nA and −0.5 V bias. The smoothed UPS spectrum of NiOEP was obtained from a 4 nm film on flame-annealed gold.

convenience, UPS spectra are reported as binding energies relative to the Fermi energy. On the basis of UPS measurements of the clean Au(111) and the flame-annealed gold substrates, work functions ϕ were determined to be 5.20 ± 0.15 eV and 4.70 ± 0.15 eV, respectively. The value for the Au(111) film 5.2 eV is in good agreement with values found in the literature for Au (111).[39] These values of work function were used to convert measured binding energies of NiOEP films to vacuum state referenced values.

Figures 7 provides the raw UPS data obtained from a 4 nm film of NiOEP deposited onto flame-annealed gold. The *x*-axis is the energy below the Fermi energy in eV. Figure 8 shows spectral data in the region near the Fermi energy at higher resolution and with the energy given relative to the vacuum level (ionization energy). To make this conversion, we added the measured Fermi energy (4.7 eV) of the flame-annealed gold substrate to the binding energy relative to E_F. Fitting the spectrum in Figure 7 to a background polynomial plus two Gaussians yields two bands in the energy range shown having peaks at 6.34 and 6.8 eV. These peaks are in reasonable agreement with the gas-phase UPS bands reported by Khandelwal and Roebber at 6.25 and 6.53 eV for H_2OEP,[40] and by Westcott et al.[41] at 6.32 and 6.76 eV for VO(OEP). An additional intense band near 7.5 eV in the gas-phase spectrum of H_2OEP probably corresponds to the 8.1 eV thin film band (C) in Figure 7 (seen at 3.4 eV relative to E_F). The highest occupied molecular orbitals (HOMOs), shoulder A and band B in Figure 7, are the nearly degenerate $a_{1u}(\pi)$ and $a_{2u}(\pi)$ MO's of the porphine ring. Khandelwal et al.[40] assign the highest occupied MO to be the a_{2u} for CuTPP, ZnTPP, and MgTPP, but choose the a_{1u} for NiTPP on the bases of reported EPR and optical spectra.

STM-OMTS. For quasi-resonant tunneling, where the tunneling electron loses little or no net energy to the adsorbate, we would expect the d*I*/d*V* versus V curve to reflect the local density of states for the adsorbate. Provided the total gap length is large compared to the adsorbate thickness, a peak will be seen in the d*I*/d*V*−*V* curve at voltages corresponding to the spectrum of ionization and affinity values (empty states in the case of tunneling from tip to molecule, filled states for the reverse process).[42,43] Thus, the electron affinity of the adsorbate is equal to the work function of the gold substrate minus the applied bias at which the peak in d*I*/d*V* occurs (see Figure 2). In reverse bias, the unoccupied orbitals never come into resonance with the Fermi energy and no peak due to unoccupied orbitals is seen. On the other hand, occupied orbitals can be brought into resonance with the tip Fermi surface only when an appropriate negative bias is applied. *Thus, both occupied and unoccupied orbitals can be probed by OMTS.* In STM d*I*/d*V* spectra, orbital-mediated tunneling OMT results in simple peaks whose band maxima correspond to orbital positions relative to the Fermi energy (e.g., Δ_r and Δ_o relative to E_F in Figure 2).

In this picture, we have assumed that the majority of the potential drop between tip and substrate occurs in the vacuum gap between NiOEP and the tip. In fact, all of the spectroscopic data was collected with a junction resistance of greater than 2 GΩ to ensure that this would be the case. As the tip−molecule separation is decreased, more and more of the voltage drop can occur across the molecular layer until, at the point of contact, one would expect a mean potential of only half the applied one.[44,45,46] Moreover, there would be no distinction between tip and substrate electrode and oxidation or reduction bands would appear in both bias directions.[13,44−46] The marked bias asymmetry and the agreement between UPS and STM-OMTS seen in Figure 8 justify our setting the NiOEP potential to that of the Au/NiOEP interface. Nevertheless, the distance dependence of the position of the maximum in d*I*/d*V* is of considerable fundamental interest. We are currently exploring this relationship, but will not further address the issue in this article.

Figure 9 presents the OMTS obtained from NiOEP (this work) and from CoTPP (ref 24) on Au (111) with a tungsten tip in the STM environment. As might be expected, the transient ring reduction and oxidation peaks (tunneling via LUMO and HOMO of the porphyrin ring, respectively) occur at similar energies for tetraphenylporphyrin and for octaethylporphyrin. The first ring ionization of both complexes occurs near −1.19 V sample bias ($\Delta_o = 1.19$). The first ring reduction (Δ_r) for the TPP ring occurs near 1.7 V bias, while that for OEP is near 1.8 V. The STM-OMTS of NiOEP seen in Figure 9 is simpler than that of CoTPP. The CoTPP spectrum has a well-defined band

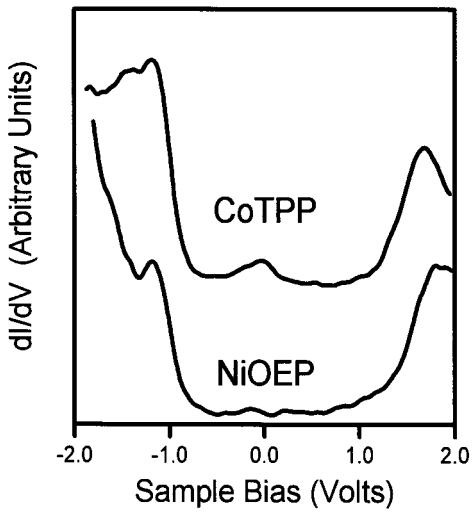

Figure 9. STM-based orbital-mediated tunneling spectra of NiOEP and CoTPP. Both curves were the result of averaging more than 10 d*I*/d*V* curves and then filtering with a Gaussian filter of width 0.1 V.

near −0.2 V bias (Δ_o = 0.2 V) that is absent in the NiOEP spectrum. This band is due to the transient oxidation of Co(II) to Co(III) through the d_{z^2} orbital.[24]

The assignment of the ring ionization band is significantly strengthened by plotting the UPS spectrum of NiOEP on the same energy scale as the STM-OMTS spectra, as seen in Figure 8. The UPS and STM-OMTS are in excellent agreement and allow assignment of the bands near 6.34 and 6.8 eV ionization energy as due to the two highest occupied porphyrin ring orbitals: the $a_{1u}(\pi)$ and $a_{2u}(\pi)$ MO's. It is the resonance like tunneling through these orbitals that provides the primary contrast mechanism for the OEP rings seen in Figure 6. The ethyl groups are also observed with good contrast because they are both physically taller, and because of the strong electronic interaction between the ethyl groups and the OEP π and π^* states noted in the resonance Raman study of Li and co-workers.[31]

In previous publications we have used an electrochemical model to estimate the positions of OMTS bands.[24,27,47,48] We found that the reduction potentials closely correlated with the first (positive bias) OMTS bands in a number of compounds. We also observed that metal centered oxidation generally differed from the predicted values by a few tenths of a volt and that the deeper ring oxidations differed significantly from the predictions of the simple model. The STM-OMTS data presented in this paper offers a further opportunity to test that model since we observe both oxidation and reduction potentials spread over about 3 V in potential. In our model, the first ionization energy and first electron affinity level of thin films supported on metals should be approximately given by the 1st electrochemical oxidation and reduction potentials, respectively.[47,48] To convert potential relative to sce to values referenced to the vacuum level, we add 4.7 V to the electrochemical values as shown in Figure 2.[29] On the bases of the results from electrochemical measurements on H_2OEP and CoOEP, we would expect the first ring reduction to occur near −1.5 V (sce), or 3.2 V below the vacuum level.[49] This is in good agreement with the value of 3.4 V observed by STM-OMTS. The first ring oxidation in solution might lie as deep as +1 V (sce), or near 5.7 eV below the vacuum level. Thus, the first oxidation in the thin film lies 0.7 V deeper than in solution. This is a large error that cannot be easily explained away. Thus, it again appears that the electrochemical model is more appropriate for estimating electron affinity levels than for ionization energies.

The failure of the transferability of electrochemical values to thin film values for oxidation processes but not reduction processes indicates that the polarization energy terms do not simply depend on sign (as supposed in Figure 2). In fact, the simple dielectric medium model that produces Figure 2 clearly does not work for these porphyrins. On the basis of the polarization stabilization of ions by the surrounding molecules and image charges induced in the metal substrate, we would expect the ionization potential of thin film NiOEP to be about 0.5 to 1.0 eV greater than for the gas phase. Instead, the ionization energies measured from a thin film are nearly identical to those reported from the gas phase.[40,41]

Armstrong and co-workers have also noticed this difficulty in reconciling solution phase oxidation potentials with thin film UPS data.[50,51] Rather than use the simple formula that results from Figure 2, $I_1 = 4.71\text{ eV} + E^{ox}(\text{sce})_{1/2}$, he finds that multiplication of the oxidation potential by a factor of about 1.7 is necessary to bring UPS HOMO peaks and solution phase electrochemical first oxidation potentials into agreement. An explanation for the physical origin of this scaling effect was not provided. It is interesting to note that if one takes the first solution phase ring oxidation to be located at +1.0V (sce), then the peak we observe in the NiOEP HOMO using Armstrong's scaled equation is I_1= 4.71 eV +1.7 eV = 6.4 eV, in very good agreement with our observed STM-OMTS peak.

Conclusions

Thin films of NiOEP on gold were studied by XPS, RAIR, UPS, STM imaging, and STM-based orbital-mediated tunneling spectroscopy. XPS and RAIR data demonstrate that NiOEP can be vapor deposited onto gold without changes in composition or oxidation state. The UPS results give the position of the highest occupied π MO's, but do not reveal the location of the lowest energy unfilled molecular orbital (LUMO). In the STM environment, high-energy π occupied orbitals and the lowest energy unoccupied π^* orbital were observed. Thus, in the region of the Fermi energy, STM-OMTS allows the determination of both filled and unfilled orbitals and in general has more information than UPS. It appears that a previously proposed electrochemical model is more appropriate for estimating electron affinity levels than for ionization energies and a modification that significantly improves the fit is discussed. The high-resolution constant current STM images provide submolecular resolution and demonstrate that the ethyl group conformation is such as to maximize the porphyrin−gold contact area.

Acknowledgment. We thank the National Science foundation for support in the form of Grants CHE 9709273 and CHE 9819318. Acknowledgment is also made to the donors of the Petroleum Research Fund administered by the ACS.

References and Notes

(1) Collman, J. P.; Halbert, T. R.; Suslick, K. S. *Metal Ions in Biology;* Spiro, T. G., Ed.; Wiley: New York, 1980; Vol. 2, p 1.

(2) Unger, E.; Beck, M.; Lipski, R.; Dreybodt, W.; Medforth, C. J.; Smith, K.; Schweitzer-Stenner, R. *J. Phys. Chem. B* **1999**, *103*, 10022.

(3) Pendergast, K.; Spiro, T. G. *J. Am. Chem. Soc.* **1992**, *114*, 3793−3901.

(4) Piffat, C.; Melamed, D.; Spiro, G. *J. Phys. Chem.* **1993**, *97*, 7441.

(5) Jentzen, W.; Unger, E.; Song, X.; Jia, S.; Tyek, I. T.; Stenner, R. S.; Draybrodt, W.; Scheidt, W. R.; Shelnutt, J. A. *J. Phys. Chem. A* **1997**, *101*, 5789.

(6) Jones, D.; Hinman, A. S. *J. Chem. Soc., Dalton Trans.* **1992**, 1503.

(7) Paolesse, R.; Di Natale, C.; Dall'Orto, V.; Macagnano, A.; Angelaccio, A.; Motta, N.; Sgarlata, A.; Hurst, J.; Rezzano, I.; Mascini, M.; D'Amico, A. *Thin Solid Films* **1999**, *354*, 245.

(8) Atamian, M.; Donohoe, R. J.; Lindsey, J. S.; Bocian, D. F.*J. Phys. Chem.* **1989**, *93*, 2236.
(9) Duong, B.; Arechabaleta, R.; Tao, N. J. *J. Electroanal. Chem.* **1998**, *447***,** 63.
(10) Kunitake, M.; Batina, N.; Itaya, K. *Langmuir* **1995**, *11*, 2337.
(11) Ogaki, K.; Batina, N.; Kuniake, M.; Itaya, K. *J. Phys. Chem.* **1996**, *100*, 7185.
(12) Kunitake, M.; Akiba, U.; Batina, N.; Itaya, K. *Langmuir* **1997**, *13*, 1607.
(13) Han, W.; Durantini, E. N.; Moore, T. A.; Moore, A. L.; Gust, D.; Rez, P.; Letherman, G.; Seely, G.; Tao, N.; Lindsay, S. M. *J. Phys. Chem. B* **1997**, *101*, 10719.
(14) Tao, N. J. *Phys. Rev. Lett.* **1996**, *76*, 4066.
(15) Tao, N. J.; Cardenas, G.; Cunha, F.; Shi, Z. *Langmuir* **1995**, *11*, 4445.
(16) Palacin, S.; Ruaudel-Teixier, A.; Barraud, A. *J. Phys. Chem.* **1986**, *90*, 6237.
(17) Shimazu, K.; Takechi, M.; Fugii, H.; Suzuki, M.; Saiki, H.; Yoshimura, T.; Uosaki, K. *Thin Solid Films* **1996**, *273*, 250.
(18) Thomas, P.; Berovic, N.; Laitenberger, P.; Palmer, R.; Bampos, N.; Sanders, J. *Chem. Phys. Lett.* **1998**, *294*, 229
(19) Furukawa, M.; Tanaka, H.; Sugiura, K.; Sakata, Y.; Kawai, T. *Surf. Sci.* **2000**, *445*, L58.
(20) Yangi, H.; Ashida, M.; Harima, Y.; Yamashita, K. *Chem. Lett.* **1990**, 385.
(21) Jung, T. A.; Schlittler, R. R.; Gimzewski, J. K.; Tang, H.; Joachim, C. *Science* **1996**, *271*, 181.
(22) Gimzewski, J. K.; Jung, T. A.; Cuberes, M. T.; Schlittler, R. R. *Surf. Sci.* **1997**, *386*, 101.
(23) Scudiero, L.; Barlow, D. E.; Hipps, K. W. *J. Phys. Chem B* **2000**, *104*, 11899.
(24) Scudiero, L.; Barlow, D. E.; Mazur, U.; Hipps, K. W. *J. Am. Chem. Soc.* **2001**, *123*, 4073.
(25) Lu, X.; Hipps, K. W. *J Phys. Chem. B* **1997**, *101*, 5391.
(26) Lu, X.; Hipps, K. W.; Wang, X. D.; Mazur, U. *J. Am. Chem. Soc.* **1996**, *118*, 7196.
(27) Barlow, D.; Hipps, K. W. *J. Phys. Chem. B* **2000**, *104*, 2444.
(28) Cullen, D.; Meyer, E. F. *J. Am. Chem. Soc.* **1974**, *96*, 2095−2102.
(29) Richardson, D. E.; *Inorg. Chem.* **1990**, *29*, 3213.
(30) Barth, J. V.; Brune, H.; Ertl, G.; Behm, R. J. *Phys. Rev. B*, **1990**, *42*, 9307.
(31) Li, X.; Czernuszewicz, R. S.; Kincaid, J. R.; Stein, P.; Spiro, T. G. *J. Phys. Chem.* **1990**, *94*, 47.
(32) Ogoshi, H.; Masai, N.; Yoshida, Z.; Takemoto, J.; Nakamoto, K. *Bull. Chem. Soc. Jpn.* **1971,** *44*, 49.
(33) Kincaid, J. R.; Urban, M.; Watanabe, T.; Nakamoto, K. *J. Phys. Chem.* **1983**, *87*, 3096.
(34) Jones, D.; Hinman, A. S. *J. Chem. Soc., Dalton Trans.* **1992**, 1503.
(35) Atamian, M.; Donohoe, R. J.; Lindsey, J. S.; Bocian, D. F. *J. Phys. Chem.* **1989**, *93*, 2236.
(36) Karweik, D. H.; Winograd, N. *Inorg. Chem.* **1976**, *15*, 2336.
(37) Muralidharan, S.; Hayes, R. G. *J. Chem. Phys.* **1979**, *71*, 2970.
(38) Niwa, Y. *J. Chem. Phys.* **1975,** *62*, 737.
(39) *Handbook of Chemistry and Physics*, 70th ed.; CRC Press: Boca Raton, 1989; p E93.
(40) Khandelwal, S. C.; Roebber, J. L. *Chem. Phys. Lett.* **1975** *34*, 355.
(41) Westcott, B. L.; Gruhn, N.; Michelsen, L.; Lichtenberger, D. *J. Am. Chem Soc.* **2000**, *122* 8083.
(42) Hipps, K. W.; Mazur, U. *J. Phys. Chem. B.* **2000**, *104*, 4707.
(43) Hamers, R. J. *J. Phys. Chem.* **1996**, *100*, 13103.
(44) If the electroactive layer is thick or separated from both electrodes, this is not the case. For example, see: Sumi, H. *J. Phys. Chem. B* **1998**, *102*, 1833 or references therein.
(45) Snyder, S. R.; White, H. S. *J. Electroanal. Chem.* **1995**, *394*, 177.
(46) Datta, S.; Tian, W.; Seunghun, H.; Reifenberger, R.; Henderson, J.; Kubiak, C. *Phys. Rev. Lett.* **1997**, *79*, 2530.
(47) Mazur, U.; Hipps, K. W. *J. Phys. Chem. B* **1999,** *103*, 9721.
(48) Mazur, U.; Hipps, K. W. *J. Phys. Chem.*, **1995**, *99*, 6684.
(49) Dolphin, D., Ed. *The Porphyrins Physical Chemistry: Part C*; Academic Press: New York, 1978; pp 142−144.
(50) Schlettwein, D.; Armstrong, N. R. *J. Phys. Chem.* **1994**, *98*, 11771.
(51) Schmidt, A.; Armstrong, N. R.; Goeltner, C.; Mullen, K. *J. Phys. Chem.* **1994**, *98*, 11780.